UC Berkeley
UC Berkeley Previously Published Works

Title

Microstructural Effects on the Interfacial Adhesion of Nanometer-Thick Cu Films on Glass Substrates: Implications for Microelectronic Devices.

Permalink

https://escholarship.org/uc/item/1ns4r65d

Journal

ACS Applied Nano Material, 4(1)

Authors

Lassnig, Alice
Terziyska, Velislava
Zalesak, Jakub
et al.

Publication Date

2021-01-22

DOI

10.1021/acsanm.0c02182

Peer reviewed

eScholarship.org
Powered by the California Digital Library
University of California

This is an open access article published under a Creative Commons Attribution (CC-BY) License, which permits unrestricted use, distribution and reproduction in any medium, provided the author and source are cited.

ACS APPLIED NANO MATERIALS

www.acsanm.org Article

Microstructural Effects on the Interfacial Adhesion of Nanometer-Thick Cu Films on Glass Substrates: Implications for Microelectronic Devices

Alice Lassnig,* Velislava L. Terziyska, Jakub Zalesak, Tanja Jörg, Daniel M. Toebbens, Thomas Griesser, Christian Mitterer, Reinhard Pippan, and Megan J. Cordill

Cite This: ACS Appl. Nano Mater. 2021, 4, 61−70

Read Online

ACCESS | Metrics & More | Article Recommendations | Supporting Information

ABSTRACT: Improving the interface stability for nanosized thin films on brittle substrates is crucial for technological applications such as microelectronics because the so-called brittle−ductile interfaces limit their overall reliability. By tuning the thin film properties, interface adhesion can be improved because of extrinsic toughening mechanisms during delamination. In this work, the influence of the film microstructure on interface adhesion was studied on a model brittle−ductile interface consisting of nanosized Cu films on brittle glass substrates. Therefore, 110 nm thin Cu films were deposited on glass substrates using magnetron sputtering. While film thickness, residual stresses, and texture of the Cu films were maintained comparable in the sputtering processes, the film microstructure was varied during deposition and via isothermal annealing, resulting in four different Cu films with bimodal grain size distributions. The interface adhesion of each Cu film was then determined using stressed Mo overlayers, which triggered Cu film delaminations in the shape of straight, spontaneous buckles. The mixed-mode adhesion energy for each film ranged from 2.35 J/m^2 for the films with larger grains to 4.90 J/m^2 for the films with the highest amount of nanosized grains. This surprising result could be clarified using an additional study of the buckles using focused ion beam cutting and quantification via confocal laser scanning microscopy to decouple and quantify the amount of elastic and plastic deformation stored in the buckled thin film. It could be shown that the films with smaller grains exhibit the possibility of absorbing a higher amount of energy during delamination, which explains their higher adhesion energy.

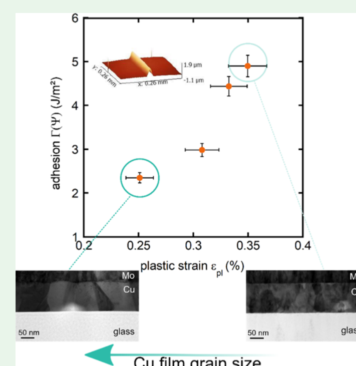

KEYWORDS: *thin film adhesion, brittle−ductile interface, spontaneous buckles, film microstructure, nanosized Cu films*

1. INTRODUCTION

Nanosized metal films are ubiquitous in various technological applications and act as coatings, protective layers, or integrated structures in microelectronic devices. Therefore, a large variety of ductile thin-film brittle substrate material combinations exist. Their mechanical behavior and involved plasticity mechanisms have been of interest for the past decades.[1] Particular focus was set on the mechanical characterization and dislocation activities of thin films on rigid substrates.[2] It is well-known that brittle−ductile interfaces are usually mechanically weak, and they often represent limitations in technological applications. Considering this, interface adhesion is an important measure to quantify the stability of the material combination and to assess the overall reliability of the system. Another approach in interface engineering is to tune the film properties to improve the interface stability. It is therefore crucial to understand how the film properties may influence their adhesion behavior.

In general, the (thermodynamical) true work of adhesion, W_{ad}, determines how energetically favorable the separation of two materials, numbered 1 and 2, attached to each other is.[3] This approach is described by the energy balance of the free surface energies of both materials, γ_i, reduced by their combined interface energy, γ_{12}, and is consistent with Griffith's crack propagation criterion for linear elastic monolithic materials, leading to the following expression[4,5]

$$W_{ad} = \gamma_1 + \gamma_2 - \gamma_{12} \quad (1)$$

Evans et al. have already recognized that these models need to be modified when a ductile component is present, as there may be some significant energy dissipation attributed to the formation of a plastic zone at the crack tip, leading to an overestimation of the true adhesion.[6,7] Experimentally, only the practical work of adhesion, Γ, is obtained and can be

Received: August 20, 2020
Accepted: December 4, 2020
Published: December 28, 2020

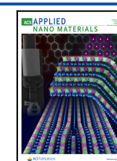

understood as the sum of two contributions: the "true" thermodynamic work of adhesion, W_{ad}, and the inelastic contributions, leading to energy dissipation mechanisms occurring at or near the interface during delamination W_p.[8]

$$\Gamma = W_{ad} + W_p \quad (2)$$

The energy balance in eq 2 necessary to cause interface delamination has been expressed similarly in previous works and depends on various extrinsic and intrinsic factors such as mode mixity, residual stresses, film thickness, interface chemistry, and film microstructure.[3,9−12]

The mixity of loading modes, defined as the mode I to mode II loading ratio at the crack tip, is often referred to as the phase angle of loading, Ψ. It has a high influence on the energy dissipation (adhesion values). When a pronounced shear loading (mode II) occurs, higher adhesion is measured than in pure mode I loading. In the case of a crack propagating at an interface between two dissimilar materials, mode mixity will always be present because of an elastic mismatch between the film and substrate materials, which can be evaluated by the Dundurs parameters.[1,3,13] Residual stresses are inevitable in thin-film systems and originate because of the deposition process, growth conditions, thermal mismatch between the involved materials, or a combination thereof. In ductile thin-film systems, residual stresses highly influence the yield behavior of the film, which in turn enhances the plasticity dissipation contribution, manipulating the interface fracture behavior significantly. For example, Litteken et al. showed that the interface fracture energy varied drastically as a function of the biaxial film stress state. Films with high compressive stress revealed 50% higher interface fracture energies compared to the same material systems with films having tensile stresses.[14] The film thickness influences the plasticity mechanisms activated within the layer and consequently determines the yield behavior of thin films and multilayers.[15] A quantification of the plastic zone size created ahead of a crack propagating at the interface allows to understand the interface fracture behavior and involved mechanisms activated during this process. In a previous study, Cordill et al. investigated the role of the microstructure of 1−2 μm thick Cu films on their adhesion to W films, finding that softer Cu films (with larger grains) adhered better to the W films as opposed to their small-grained counterparts. A quantification of the plastic zone size next to the delaminated regions revealed that films with stronger adhesion were accompanied by larger plastic zones.[16] However, a detailed analysis of how the microstructure of nanosized metallic films influences interface adhesion is still lacking. A change in the interface chemistry due to interfacial reactions (e.g., interdiffusion of the materials) can lead to the degradation and aging of the interface properties because of the creation of bulk interfaces. A highly feared example in microelectronics is bulk copper silicides (e.g., Cu_3Si), which form when Cu films are directly deposited on silicon.[17,18] However, for polymer substrate metal films also, bulk interfaces were found to change the interfacial structure significantly when the material system is exposed to elevated temperatures.[19] The glass−Cu system reveals adhesion values around 2 J/m^2 obtained by a double cantilever beam (DCB) test method. The fracture location of this materials system is the interface; a plastic zone size of around 0.31 μm accompanying the delamination has been found for Cu films with a thickness of around 100 μm.[20] By introducing controlled interfacial geometries, a significant improvement of the same interface could be achieved by a factor of 4−7 by designing novel interface geometries and benefiting from extrinsic toughening.[21] The authors state that plasticity in the Cu film is responsible for the improved interfacial toughness.

Various factors influence the adhesion behavior of the investigated materials system. Usually, these factors (residual stress, interfacial reactions, film thickness, and microstructure of a film) are difficult to decouple from each other. The model of Hutchinson and Suo for straight-sided buckles has been widely adopted to quantify the interfacial fracture energy of bimaterial interfaces,[22] allowing to easily assess the adhesion data of thin films, which delaminate in the shape of straight-sided buckles. This model is, however, rooted in the Euler beam theory and assumes elastic deformations while ignoring plastic deformation during the delamination. Plasticity is known to play an important role during delamination, but the early research mostly dealt with film thickness effects rather than film microstructural effects.[23,24] Recently, theoretical work has been dedicated to account for dislocation activity during delamination by Ruffini and coworkers.[25,26]

Within this study, it is the goal to decouple film microstructure from the abovementioned parameters and to thoroughly study its influence on interface adhesion energy for nanometer-sized films. Therefore, thin Cu films were deposited on glass substrates by means of DC magnetron sputtering. This model system was chosen because no bulk interphases between Cu and glass are expected to form during deposition and after heat treatments. The adhesion was determined using stressed Mo overlayers deposited on top of the Cu films causing, delamination of the Cu−glass interface. This method was chosen because it is easy to perform on very thin films in the nanometer regime, allowing to locally assess adhesion of the desired interface.[27,28]

2. EXPERIMENTAL DETAILS

2.1. Investigated Materials. Copper thin films with a thickness of 110 nm were sputter-deposited onto 0.5 mm thick boroaluminosilicate glass substrates (Corning EAGLE2000 AMLCD). The films were deposited in a lab-scale magnetron sputtering device by sputtering from one Cu target (purity of 99.99%, dimensions of Ø 50.8 mm × 6 mm), where the distance between the target and substrate was 4.5 cm. During deposition, the DC current applied to the Cu target was set to 0.4 A while an asymmetric bipolar pulsed DC bias voltage of −100 V was applied to the substrate. Two deposition runs were performed at 0.5 and 1 Pa argon pressures (corresponding to Ar flows of 30 and 60 sccm, respectively) without additional substrate heating for around 1 min deposition time. The change of argon pressure during deposition resulted in two Cu films with different initial microstructures but having the same thickness. A further modification of the film microstructure could be achieved by isothermal annealing under vacuum at 400 °C (corresponding to a homologous temperature of Cu of around $T_h \sim 0.5$) for 2 h. The study was conducted on both the as-deposited and annealed films, leading to a total of four different film microstructures.

The grain size distribution of the film surface was quantified using ion channeling contrast (ICC) imaging in a Zeiss LEO 1540XB focused ion beam (FIB) workstation. The average grain diameter of the coarse grains and the area percentage of the nanosize-grained regime was determined from the obtained images, followed by a particle size analysis with DigitalMicrograph. Twins eventually formed within the Cu grains are not considered in this study.

The film cross sections were also examined with transmission electron microscopy (TEM) for which electron transparent lamellae were prepared in an FEI Helios NanoLab 660 FIB workstation equipped with an FEI EasyLift EX micromanipulator. Rough and fine cutting was conducted at an accelerating voltage of 30 kV, and milling currents ranged from 20 nA to 50 pA. The final polishing of the lamellae was performed at an accelerating voltage of 5 kV and milling current of 50 pA. The TEM sample preparation was conducted on samples covered with a protective Mo overlayer (described later); thus, the Cu films were protected during the entire sample preparation process. The specimens were observed in a JEOL 2200 FS TEM using an acceleration voltage of 200 kV. For a better grain contrast, the images were taken in bright-field scanning transmission electron microscopy (BF-STEM) mode.

After a detailed analysis of the Cu films in the as-deposited and annealed state was conducted, stressed Mo overlayers were deposited with high compressive stresses to cause controlled delaminations at the Cu−glass interface. An industrial scale in-line magnetron sputtering system with a rotatable Mo target (FHR Line. 600 V, target size ϕ 152 mm × 600 mm) was used.[29] Prior to deposition, an inverse sputter-etching step was introduced to remove possible oxides and debris on the Cu films and to ensure good adhesion between the Cu films and the Mo SOL. The Cu film samples were fixed on the carrier, and after a pressure of less than 1 × 10^{-4} Pa was reached, a gate valve opened, and they were moved into the deposition chamber. Sputter-etching was conducted by oscillating the carrier for six cycles with a velocity of 20 mm/s in front of an radiofrequency plasma with an argon pressure of 0.28 Pa and a power of 0.8 kW. For the deposition, the carrier was stationed in a central position opposite to the magnetron at a target−substrate distance of 75 mm. The Mo SOL was deposited on the Cu films with a discharge power of 10 kW, an Ar pressure of 0.37 Pa, and 10 rotations per minute of the target. The entire sputter process lasted 46 s, leading to 500 nm thick Mo SOL with a high compressive residual stress of −2.2 GPa, which was measured by XRD using the 110 peaks of the Mo films, as described in Section 2.2.

Figure 1 shows a schematic of the investigated structure. The high compressive stress induced spontaneous delamination at the Cu−glass interface in the form of straight-sided buckles. From these resulting buckles, the interface fracture energy, or adhesion, could then be measured using the adhesion mechanics presented in Section 2.3.

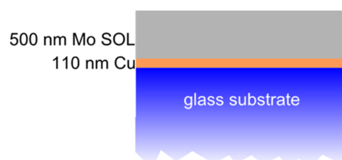

Figure 1. Schematic of the film system: glass substrates covered with 110 nm thin Cu films with highly stressed Mo overlayer on top for adhesion measurements.

2.2. Residual Stresses and Yield Stress Estimation of Cu Films. The residual stresses in the four different copper films (as-deposited and annealed) were determined by synchrotron radiation (KMC-2 beamline, BESSY II, Berlin) using a Bruker VÅNTEC 2000 detector.[30] The film strains were determined by means of the $\sin^2 \Psi$ method, where 111 and 200 Cu peaks were recorded at nine different φ angles between 0 and 50°. An exposure time of 7 s and a beam energy of 8048 eV (wavelength 0.154 nm, equivalent to Cu Kα_1) were used. Directional stress inhomogeneities were excluded by repeating the experiments with the specimen rotated 90° around its surface normal. The peak positions and widths were then acquired using Pearson fits, revealing the obtained lattice strains. The corresponding X-ray elastic constants for the recorded Cu peaks were then determined by means of the Elastix database assuming the Hill model,[31] allowing to finally compute the film stresses.

Nanoindentation was also performed on the Cu films to estimate their yield stresses. Using a Bruker TS77 Select nanoindenter with a Berkovich tip (approximate radius of 200 nm), 25 indents were made using loads between 100 and 1500 μN (resulting in displacements between 20 and 100 nm, respectively) and a constant loading rate. Residual indent imprints were larger than the average grain size of the films. The indent load−displacement curves were analyzed using the well-known Oliver and Pharr method and an area function calibrated using fused silica.[32] From the evaluated hardness measurements and Tabor's solution ($H = 2.8\sigma_y$, H is the hardness and σ_y is the yield stress), the yield stress of the Cu films were estimated.[33]

2.3. Adhesion Mechanics. Adhesion was determined from the spontaneous buckles caused by the Mo SOL, as described by previous works.[34−36] Bagchi and Evans have built the frameworks on the mechanics of bilayer delamination from a substrate;[37] Kriese et al. extended the model to include indentation-induced delamination of bi- and multilayer systems.[35,38] The characteristic dimensions of the buckles allow to determine the interfacial fracture energy, $\Gamma(\Psi)$. For bilayer delamination, the model of Hutchinson and Suo for straight-sided spontaneous buckles can be extended by including the different stiffnesses of the involved film materials.[22] The critical buckling stress, σ_B, can then be determined by computing the moment of inertia, I_T, of this bilayer system, according to[35,38]

$$I_T = \sum_{i=1}^{2} \frac{1}{12} n_i k h_i^3 + n_i k h_i (\overline{Y} - y_i)^2 \quad (3)$$

where $\overline{Y}$ is the composite centroid, considering the different moduli, E_i, of the films, y_i, is the centroid, and, h_i, is the film thickness of each individual layer, respectively. In eq 3, n is necessary to create a transformed cross section of the two layers taking the different Young's moduli of the investigated materials into account. The variables k and b will cancel out once the critical buckling stress, σ_B, is computed with eq 4. For a deeper understanding, the reader is referred to ref 35.

The critical buckling stress, σ_B, can be obtained by

$$\sigma_B = \frac{\pi^2}{khb^2}\left[\frac{E_1}{1 - \upsilon_1^2}\right] \cdot I_T \quad (4)$$

where E_1 is the Young's modulus, and ν_1 is the Poisson's ratio of the Mo film (material 1 of the layer system).

The residual or driving stress, σ_D, is then analogous to the model of Hutchinson and Suo

$$\sigma_D = \sigma_B \cdot \left[\frac{3}{4} \cdot (\delta/h)^2 + 1\right] \quad (5)$$

where δ is the buckle height and h is the total film thickness of the involved layers.[22]

Finally, the mixed-mode adhesion energy $\Gamma(\Psi)$ can be computed analogously to straight-sided buckles[22]

$$\Gamma(\Psi) = \left[\frac{(1 - \nu^2)h}{2E}\right](\sigma_D - \sigma_B)(\sigma_D + 3\sigma_B) \quad (6)$$

where h is the total film thickness, E is the thickness weighted modulus, and ν is the thickness weighted Poisson's ratio of the bilayer. The phase angle of loading, Ψ, corresponds to the ratio of mode I and II loading modes and can be estimated by eq 7

$$\Psi = \tan^{-1}\left[\frac{4\cos\omega + \sqrt{3}\xi \sin\omega}{-\sin\omega + \sqrt{3}\xi \cos\omega}\right] \quad (7)$$

where ω is around 52.1° and $\xi = \delta/h$ corresponds to the ratio of the buckle height to the total film thickness.

The interfacial fracture toughness under pure mode I (normal forces acting at the interface) Γ_I can then be obtained by

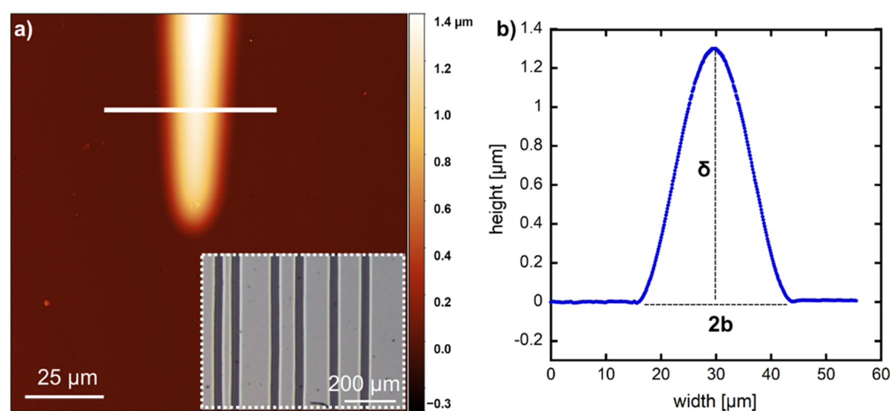

Figure 2. (a) CLSM profile imaging of a spontaneous buckle. Inset shows overview of several straight buckles throughout the sample and (b) buckle height profile corresponding to the region of interest (white line) highlighted in (a) with δ buckle height and $2b$ the buckle width indicated.

$$\Gamma_{\mathrm{I}} = = \frac{\Gamma(\Psi)}{1 + \tan^2\{(1-\lambda)\cdot\Psi\}} \quad (8)$$

where λ is a material parameter and is approximately 0.3.[39]

2.4. Postbuckling Characterizations. Spontaneous delamination of the Cu films from the glass substrates was achieved with the addition of a 500 nm Mo SOL in the shape of straight buckles, as shown in Figure 2a. The buckles were then used to compute the corresponding adhesion energies according to eqs 3−8. Confocal laser scanning microscopy (CLSM) (OLYMPUS LEXT 4100 OLS) was employed to determine the buckle dimensions (buckle height, δ, and buckle width, $2b$) as shown in Figure 2b. For the adhesion evaluation, at least three buckles per film were used and a total of at least 20 measurements were conducted. The straight-sided buckles were quite long and traversed most of the sample width (up to 1 cm), as shown in the inset in Figure 2a. The delamination morphologies were identical for each Cu film type as the buckle shape was controlled by the Mo overlayer.

The failing interface was confirmed by FIB cross-sectioning of the buckles and examination through the transparent glass substrate. A delamination of the Cu−Mo interface could be generally excluded by an optical inspection of the bottom side through the transparent glass substrate and the top side (molybdenum side) of the delaminated films, where the exact same delamination morphologies (i.e., buckles) were observed.

2.5. X-Ray Photoelectron Spectroscopy of the Cu−Glass Interface. X-Ray photoelectron spectroscopy (XPS) analyses were conducted on selected Cu−glass interfaces to check if the interfacial chemistry changes significantly as a function of (a) the deposition parameters (0.5 Pa vs 1 Pa Ar pressure) and (b) isothermal annealing of the Cu films (0.5 Pa as-deposited vs 0.5 Pa annealed). The Cu films were peeled off the glass substrates using a double-sided tape, and both parts were then immediately analyzed. The XPS spectra of both sides (the Cu film and glass substrate sides) were recorded using a Thermo Scientific instrument (K-Alpha spectrometer, Thermo Fisher Scientific, Waltham, USA) equipped with a monochromatic Al Kα X-ray source (1486.6 eV). High-resolution scans were performed with a pass energy of 50 eV and a step size of 0.1 eV. All analyses were performed at room temperature.

3. EXPERIMENTAL RESULTS AND DISCUSSION

3.1. Cu Film Characterization: Microstructure, Mechanical Properties, and Chemistry. All four films revealed a highly bimodal grain structure, where coarse grains are embedded in an ultrafine-grained matrix, as shown in the ICC images in Figure 3. After annealing, significant grain coarsening and a reduction of the ultrafine-grained regime were observed.

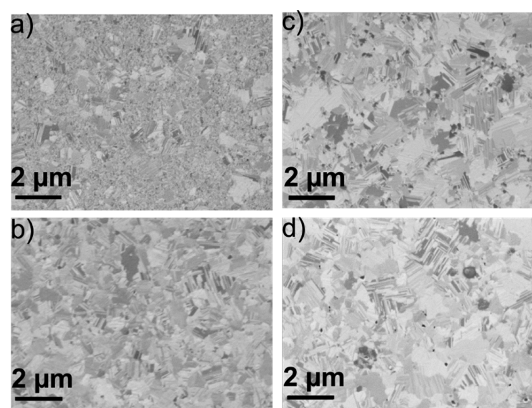

Figure 3. ICC images showing the top view of the Cu film microstructures in their as-deposited and annealed (2 h at 400 °C) states. (a) As-deposited at 0.5 Pa Ar pressure and its annealed counterpart (c); (b) as-deposited at 1 Pa Ar pressure and its annealed counterpart (d).

Using the images in Figure 3 the grain size distribution of each film type was quantified. The films deposited at 0.5 Pa Ar pressure revealed a highly bimodal microstructure: 71% of the investigated area is nanocrystalline with grain sizes of few tens of nanometers, and 29% of the area is coarse-grained with an average grain diameter of 340 nm. After isothermal annealing of the same film, the coarse-grained area fraction increased to 69%, with an average grain diameter of 352 nm. The annealing treatment did not change the average size of the coarse grains significantly but decreased the amount of the ultrafine-grained matrix. The films deposited at 1 Pa Ar pressure also showed a bimodal microstructure, where 50% of the investigated area is coarse-grained with an average grain diameter of 320 nm. After annealing, 67% of the area was covered with coarse grains with an average grain size of 463 nm. In this film system, the annealing treatment not only decreased the fraction of ultrafine-grained matrix but also increased the average size of the coarse grains significantly. A preferential texture was not detected in any of the films, as confirmed by electron backscatter diffraction (EBSD) scans in Figure 4. A summary of the grain size distributions can be found in Table 2.

BF-STEM images were also made on selected films to reveal the cross-sectional microstructure throughout the Cu film thickness and to exclude the presence of bulk interfacial phases or a drastic change of the Cu−glass interface morphology during heat treatments. Figure 5 shows the TEM cross sections of the Cu films deposited at 0.5 Pa Argon pressure in the as-deposited (fine-grained section) (a) and annealed state (b). The cross-sections agree well with the top-

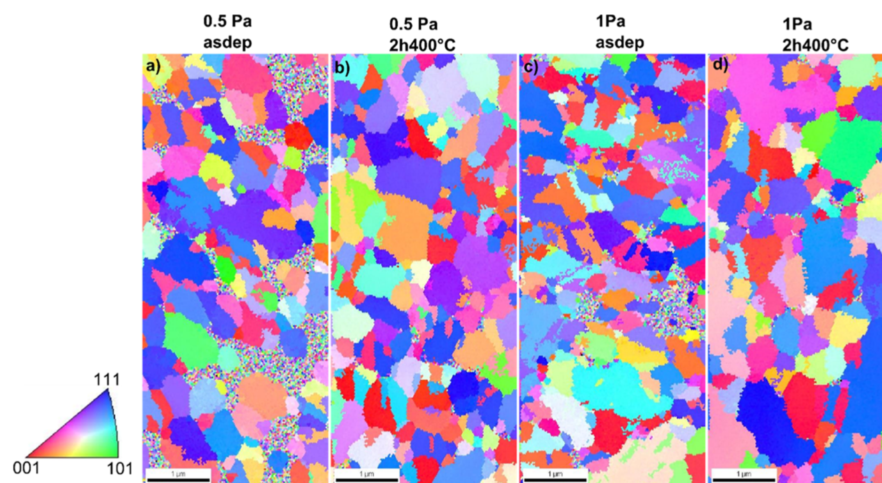

Figure 4. EBSD scans of the top view of the Cu films: films deposited at 0.5 Pa Ar pressure (a) and after annealing (b); films deposited at 1 Pa Ar pressure (c) as-deposited at 1 Pa Ar pressure and (d) after annealing.

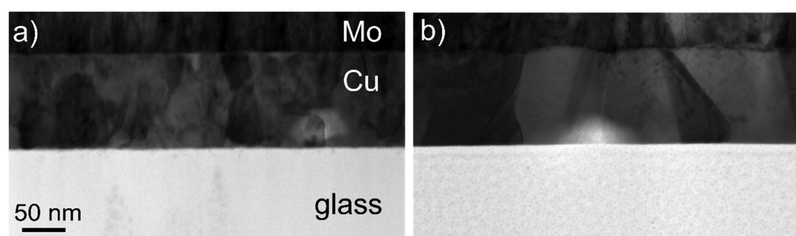

Figure 5. BF-STEM images of the Cu sample deposited at 0.5 Pa Ar pressure (a) as-deposited and (b) annealed Cu−glass interfaces covered with Mo overlayer.

Table 1. Chemical Surface Composition (at. %) of the Glass Side and Cu Film Side as a Function of the Deposition Parameter and Isothermal Annealing

	glass side (at. %)						Cu film side (at. %)			
film type	O	Si	Cu	C	Ca	N	Cu	O	C	N
0.5 Pa as-dep.	55.76	26.13	2.23	13.21	1.50	1.17	42.34	23.41	31.17	3.09
1 Pa as-dep.	56.15	26.42	1.73	13.15	1.38	1.19	42.01	23.10	32.62	2.28
0.5 Pa annealed	56.43	26.39	2.06	13.51	1.61	1.71	39.77	24.76	32.38	3.08

view images in Figure 3 and again confirm significant grain coarsening due to the annealing treatment. While the annealed films predominantly reveal columnar grains, as-deposited films have small-grained regimes and various grains throughout the film thickness. The Cu−glass interface morphology is similar in both states, and a perfectly flat interface is maintained. It can therefore be expected that annealing has no influence on bulk chemical reactions at the interface or a change in the interface roughness.

The hardness, H, of each Cu film was obtained using nanoindentation, as previously described. Tabor's solution, $\sigma_y = H/2.8$, allows the direct estimation of the yield stress, σ_Y, of each Cu film. The films deposited at 0.5 Pa Ar pressure showed a hardness of (4.13 ± 0.23) GPa and a corresponding yield stress of (1.48 ± 0.08) GPa. After annealing, hardness and yield stress dropped to (3.42 ± 0.16) GPa and (1.22 ± 0.06) GPa, respectively. For the films deposited at 1 Pa Ar pressure, a similar trend could be observed: the as-deposited films showed a hardness of (4.40 ± 0.25) GPa and a yield stress of (1.57 ± 0.09) GPa. After annealing, both values decreased to (3.50 ± 0.15) GPa and (1.25 ± 0.05) GPa, respectively. As expected, the films with a higher area fraction of the coarse-grained region and larger average grain size show decreased yield stress values. Table 1 summarizes the results of the XPS survey scans showing a similar distribution of the elements on the glass substrates and on the Cu film sides, regardless of the deposition parameter and annealing treatment. For a more detailed analysis, the Cu 2p peaks were recorded on the substrates and film sides and are summarized in Figure 6. While the spectra of the Cu films (Figure 6a) were similar for all three specimens, showing a mixture of Cu and Cu_2O; the Cu 2p peaks recorded on the glass side needed an additional peak fit analysis (Figure 6b),[40] showing an additional contribution of $Cu(OH)_2$ in the as-deposited state, which vanished in the annealed state.[41] The chemical composition is identical between both as-deposited runs. From these results, it can be demonstrated that the interface chemistry is similar for the as-deposited and annealed samples and thus does not significantly contribute to the different adhesion energies that were measured.

3.2. Residual Stresses. All four Cu films showed equi-biaxial tensile stresses. In the case of the as-deposited 0.5 Pa films, residual stresses of (120 ± 17) MPa and after annealing, an increase of the stresses up to (310 ± 24) MPa was measured. In contrast, for the 1 Pa-deposited films, the as-deposited film revealed higher tensile stresses of (321 ± 16) MPa, which slightly decreased after annealing to (229 ± 24) MPa. All four films feature tensile stresses in the MPa regime (all four were below 500 MPa), and, therefore, it is assumed that the different film stress values do not alter the mechanical behavior of the interface significantly.

3.3. Interfacial Fracture Energy Evaluation. Overall inspection of the buckled samples from the top side (Mo) and the bottom side (transparent glass) revealed the same buckling morphologies, which confirms that the delamination occurred only

https://dx.doi.org/10.1021/acsanm.0c02182
ACS Appl. Nano Mater. 2021, 4, 61−70

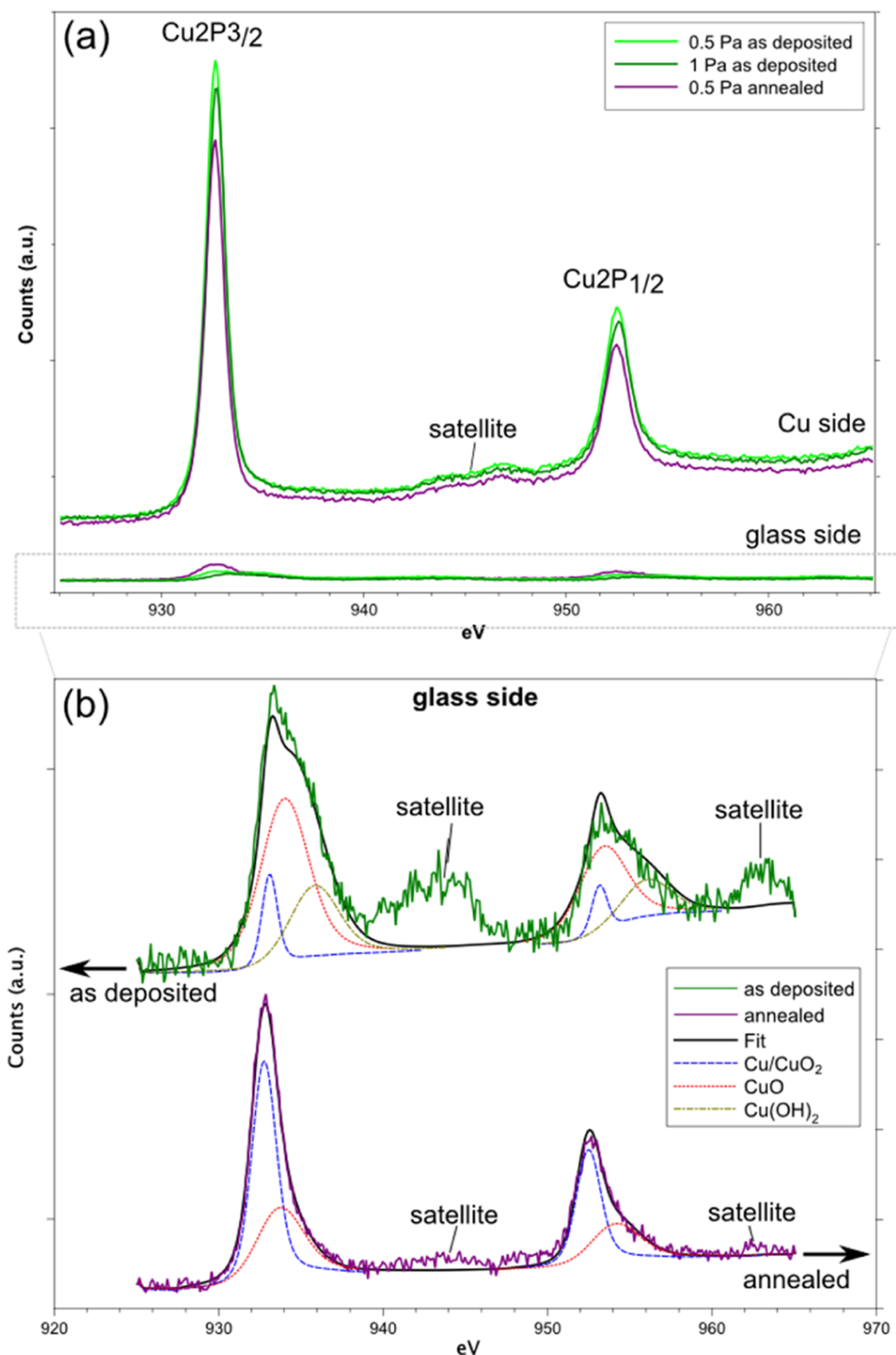

Figure 6. Cu 2p core-level XPS spectra of the as-deposited and annealed specimens with (a) overview of the Cu film and glass sides, respectively, and (b) detailed comparison of Cu 2p core-level XPS spectra derived from the peeled glass surfaces of the as-deposited and annealed samples.

at the Cu−glass interface. A delamination between the Cu film and the Mo overlayer can therefore be excluded in every specimen. FIB cross sections on selected buckles are shown in Figure 7 revealing the onset of the buckles. A similar behavior of the delaminated films for each Cu film can be observed.

Using the adhesion mechanics presented in Section 2.3 and the buckle dimensions determined by CLSM, the interfacial fracture energies were calculated for each film system. The films deposited at 0.5 and 1 Pa revealed a similar trend: the coarser grained films revealed lower adhesion energies than their small-grained counterparts. For the films deposited at 0.5 Pa, the as-deposited films revealed adhesion energies of (4.90 ± 0.33) J/m^2, and after annealing (and subsequent grain coarsening) the adhesion value decreased to (2.98 ± 0.19) J/m^2. The films deposited at 1 Pa revealed a similar behavior: in the as-deposited state, the adhesion was (4.43 ± 0.12) J/m^2; after annealing the adhesion dropped to (2.35 ± 0.12) J/m^2. The films with a higher amount of nanosized grains and a smaller average grain size revealed higher adhesion energies compared to the films with larger grains, while other parameters, such as film thickness and residual stresses remained comparable. For each buckle type, the corresponding Ψ angle of loading was computed ranging between −80 and −87°, which indicates a dominant shear loading mode during delamination for all film types. The normal- mode adhesion energy Γ_I was also

https://dx.doi.org/10.1021/acsanm.0c02182
ACS Appl. Nano Mater. 2021, 4, 61−70

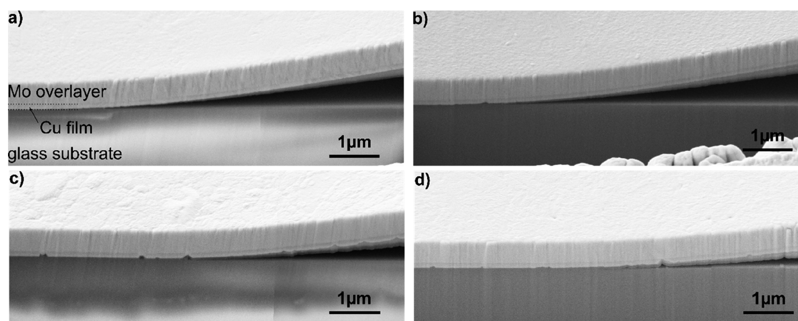

Figure 7. FIB cross sections of the delaminated films, showing the onset of the buckles: (a) film deposited at 0.5 and (b) 1 Pa, both in the as-deposited state, (c) film deposited at 0.5 Pa, after annealing, and (d) film deposited at 1 Pa, after annealing.

Table 2. Summary of Cu Thin Film Properties

film type	area fraction of nanocrystalline regime (%)	av. grain size of coarse-grained regime (nm)	residual stress (MPa)	hardness H of Cu film (GPa)	yield stress σ_Y of Cu film(GPa)	adhesion $\Gamma(\Psi)$ (J/m^2)	Ψ	Γ_I (J/m^2)
0.5 Pa as-deposited	71	340	120 ± 17	4.13 ± 0.23	1.48 ± 0.08	4.90 ± 0.33	−87°	1.14 ± 0.08
0.5 Pa annealed	39	352	310 ± 24	3.42 ± 0.16	1.22 ± 0.06	2.98 ± 0.19	−80°	0.92 ± 0.06
1 Pa as-deposited	50	320	321 ± 16	4.40 ± 0.25	1.57 ± 0.09	4.43 ± 0.12	−84°	1.17 ± 0.03
1 Pa annealed	33	463	229 ± 24	3.50 ± 0.15	1.25 ± 0.05	2.35 ± 0.12	−81°	0.70 ± 0.04

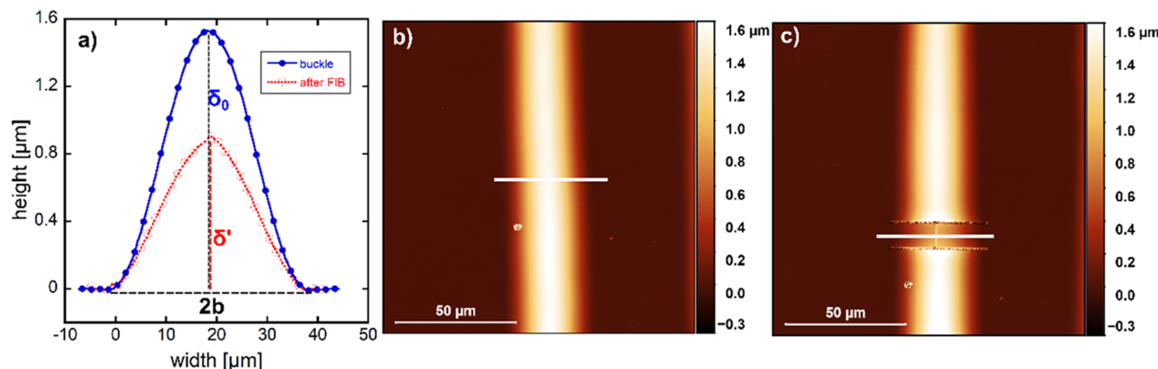

Figure 8. Profile analysis of the same buckle before and after H-shaped FIB cutting. (a) Comparison of height profiles of a buckle (before and after FIB cutting) measured from the corresponding CLSM images before (b) and after H-shape FIB cutting (c), respectively.

determined for each film type, according to eq 8. Again, the films with larger grains show lower adhesion under pure mode I loading. An overview of the results is given in Table 2. The values of the adhesion strength compare well to other values for the Cu−glass interface in literature. For example, Oh et al. measured interfacial fracture energies between 1 and 10 J/m^2 using a DCB geometry; the inherent toughness G_0, however, is in the order of 2 J/m^2.[21]

3.4. Elastic and Plastic Contribution of Buckles. Films with a higher amount of nanocrystalline grains and smaller average grain size in the coarse-grained regime show an increased mixed mode fracture energy and normal-mode adhesion, which is in contradiction to previous studies.[16,42] To shed light into the involved mechanisms during interfacial delamination and to understand why thin films with smaller grains result in higher adhesion energies, an additional study was conducted using a postbuckling FIB cut method, which allows to decouple the amount of elastic and plastic energy stored in the buckles. Therefore, two parallel cross-sectional FIB cuts across the total width of selected buckles were performed around 10 μm apart. A third cut was then positioned perpendicular to both previous cuts approximately at the point of maximum buckle height, resulting in an H-shaped FIB cut perpendicular to the buckle, as shown in Figure 8c. The investigated buckles were imaged with CLSM before and after FIB cutting to evaluate the amount of relaxation and permanent deformation due to buckling of the film system. If the buckles were purely elastic, the FIB cut part would entirely collapse and return to its original flat thin film shape. The comparison of the buckle height (Figure 8a) revealed permanently deformed buckles, with a residual buckle height, δ', being less than the original buckle height, δ_0, but having the same buckle width 2b, meaning that the interfacial crack did not propagate further than the already delaminated portion.

The comparison of the height profiles in Figure 8 reveals that after buckling, permanent deformation in the film is present. To quantify the deformation ε in the buckled Cu film, eq 9 is used to estimate the strain ε at the onset of a buckled region

$$\varepsilon = -\frac{y}{\rho}\begin{cases} \varepsilon_{e+p} = -\dfrac{y}{\rho_{\text{buckle}}} \\ \varepsilon_{pl} = -\dfrac{y}{\rho_{\text{FIB}}} \end{cases} \tag{9}$$

where y is the coordinate of the Cu film with respect to the neutral axis of the Cu−Mo bilayer system, taking the different Young's moduli and thicknesses of the individual films of the bilayer into

account. ρ corresponds to the radius of curvature at the onset of the buckle and may either be determined in the buckled state, ρ_{buckle}, or after the FIB cut, ρ_{FIB}, to determine the sum of the elastic and plastic strain in the buckled state, ε_{e+p}, or only the plastic (permanent) strain, ε_{pl}, after FIB cutting, respectively. For the computation of ρ, the reader is referred to the Appendix (see eq A2). In Figure 9 the mixed-mode adhesion energy is plotted as a function of the plastic strain ε_{pl} and the films, which showed increased adhesion also exhibited a higher plastic deformation. Therefore, the energy absorption during plastic deformation can be regarded as the main dissipation mechanism during interface delamination. The stress state of the Cu films during buckling delamination via a stressed Mo overlayer and subsequent stress relief after above described FIB cut can be understood using a stress−strain relationship in the loaded (i.e., buckled) and unloaded condition (i.e., after FIB cut). In this discussion, it is assumed that the Mo overlayer deforms purely elastically in each state. In the unbuckled state, a highly stressed Mo overlayer of −2 GPa compressive stress is deposited onto the Cu film. After buckling, the stress in the Mo overlayer is relieved, leading to a deformation of the Mo film $\varepsilon_{Mo} = \sigma/E_{Mo}$ = 2 GPa/329 GPa ≅ 0.6%. The Cu film undergoes the same deformation, which leads to a stress σ_{Cu1} proportional to its Young's modulus, E_{Cufilm}, namely, $\sigma_{Cu1} = E_{Cufilm} \times \varepsilon_{Mo}$. In addition, the Cu film experiences deformation ε_{e+p} at the onset of a buckle described by eq 9 using ρ_{buckle}. After the FIB cut, the stress of the buckle segment is relieved and only the final deformation, ε_{pl}, described by eq 9, with ρ_{FIB} present. The deformation values in the loaded and unloaded state are compared in Table 3. For the films with smaller grains, increased yield stresses were measured compared to the larger grained films. Consequently, when comparing the stress−strain curves of a large-grained and small-grained film that buckles, more energy can be absorbed by the small-grained films, which is also confirmed by the higher adhesion values.

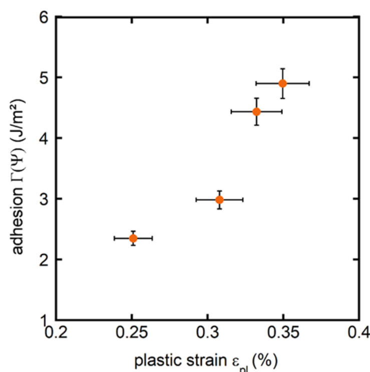

Figure 9. Adhesion vs plastic strain in Cu after buckling.

4. CONCLUSIONS

In this study, the main question was to determine if the film grain size has an influence on the adhesion values of nanosized Cu films, while other aspects such as film thickness, interface morphology and chemistry, as well as residual stresses, and loading mode of the thin films were comparable. It was shown on 110 nm Cu films on glass substrates that spontaneous delamination via a stressed overlayer is accompanied by significant plastic deformation in the Cu film, which is the most dominant energy dissipation mechanism in this material system. The as-deposited films with smaller grains revealed higher mixed mode and pure mode I adhesion values. To understand the involved dissipation mechanisms, postbuckling studies were conducted by means of a customized FIB sectioning method, allowing for the decoupling of the elastic and plastic contribution during the buckling (delamination) process. All films revealed significant plastic strains between 0.25 and 0.35% in the unloaded condition, which were quantified in the buckle onsets. These strain values were then compared to the adhesion data and illustrated a direct link between plastic deformation and the mixed-mode adhesion energy. The delamination process via buckling by means of a stressed overlayer was compared to a stress−strain curve analogy, where the buckled Cu film corresponds to the point of maximum loading, and FIB cutting leads to an unloaded, permanently deformed Cu film. In this comparison, the small-grained Cu films with increased adhesion energies also have a higher yield stress than the large-grained counterpart. Thus, the buckling of the small-grained film absorbs a higher amount of energy than the large-grained Cu film, which is consistent with the increased adhesion values. While the model of Hutchinson and Suo is rooted in elastic beam theory, it could still be employed successfully here because the experimentally obtained height profiles of the loaded and unloaded buckles could be correlated very well with the curve fit suggested by the model. The gained insights of this study open new routes in the design of multilayered structures in microelectronics applications: the film microstructure of nanosized metal films is an important parameter in interface engineering.

APPENDIX A

Determination of the Radius of Curvature

The radius of curvature ρ_0 at the onset of buckling can be computed using beam theory. The displacement of the

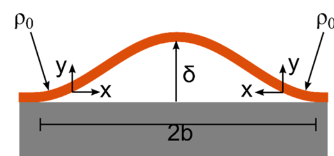

Figure A1. Coordinate system of deflection line $y(x)$ describing the buckled film to determine its radius of curvature at the onset of buckling. Redrawn with modifications after ref 43.

Table 3. Deformation of Cu Film in Loaded (Buckle) and Unloaded (after FIB Cut) Conditions as a Function of the Cu Film Microstructure Corresponding to the Mixed-Mode Adhesion Value

film type	strain loaded $\varepsilon_{total} = \varepsilon_{Mo} + \varepsilon_e + p$ (%)	plastic strain after FIB ε_{pl} (%)	yield stress of Cu film (GPa)	adhesion Γ(Ψ) (J/m²)
05 Pa as-deposited	1.30	0.35	1.48 ± 0.08	4.90 ± 0.33
05 Pa annealed	1.22	0.31	1.22 ± 0.06	2.98 ± 0.19
1 Pa as-deposited	1.31	0.33	1.57 ± 0.01	4.43 ± 0.12
1 Pa annealed	1.14	0.25	1.25 ± 0.05	2.35 ± 0.12

https://dx.doi.org/10.1021/acsanm.0c02182
ACS Appl. Nano Mater. 2021, 4, 61−70

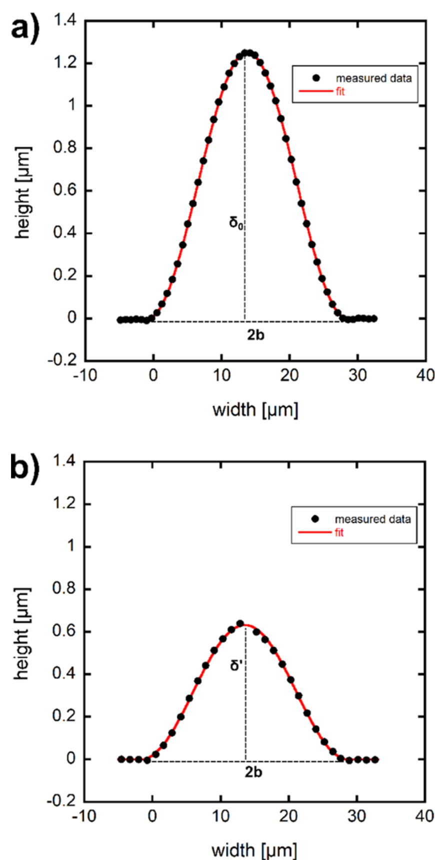

Figure A2. Curve fit for height profiles before (a) and after the FIB cuts (b) of representative buckle (data of buckled Cu film deposited at 1 Pa Ar pressure in the as-deposited state). In both cases, the buckles can be very accurately approximated by eq A3 with the characteristic buckle dimensions as parameters.

buckled film can be described by the $y(x)$-coordinates, as shown in Figure A1. The function describing the buckle can be approximated using a cosine-shaped deflection curve,[43] cf. eq A1.

$$y(x) = (\delta/2)(1 - \cos(2\pi x/2b)) \qquad \text{for } 0 \le x \le b \tag{A1}$$

The radius of curvature ρ_0 at the onset of buckling, according to Figure A1, can then be approximated by eq A2

$$\frac{1}{\rho_0} \approx \left(\frac{\partial^2 y}{\partial x^2}\right)_{x=0} \cong 2\delta(\pi/2b)^2 \tag{A2}$$

Because plastic deformation has a significant contribution in the delamination process, the validity to apply eq A1 to plastically buckled specimens was tested by fitting eq A3 to the experimentally obtained height profiles of the buckles before and after FIB cutting. The fit parameters, δ and $2b$, correspond to the measured buckle dimensions. Figure A2 visualizes how the fit and the experimentally obtained data coincide.

$$y = \frac{\delta}{2}\cdot\left(1 - \cos\left(\frac{2\pi(x + x_0)}{2b}\right)\right) \tag{A3}$$

■ ASSOCIATED CONTENT

Supporting Information

The Supporting Information is available free of charge at https://pubs.acs.org/doi/10.1021/acsanm.0c02182.

Coordinate system of deflection line $y(x)$ describing the buckled film to determine its radius of curvature at the onset of buckling (PDF)

Curve fit for height profiles before and after the FIB cuts of the representative buckle (PDF)

■ AUTHOR INFORMATION

Corresponding Author

Alice Lassnig − *Erich Schmid Institute of Materials Science, Austrian Academy of Sciences, 8700 Leoben, Austria;* orcid.org/0000-0001-6471-1635; Email: alice.lassnig@oeaw.ac.at

Authors

Velislava L. Terziyska − *Department of Materials Science, Montanuniversitaet Leoben, 8700 Leoben, Austria*

Jakub Zalesak − *Erich Schmid Institute of Materials Science, Austrian Academy of Sciences, 8700 Leoben, Austria*

Tanja Jörg − *Department of Materials Science, Montanuniversitaet Leoben, 8700 Leoben, Austria*

Daniel M. Toebbens − *Helmholtz-Zentrum Berlin für Materialien und Energie (HZB), 12489 Berlin, Germany*

Thomas Griesser − *Institute of Chemistry of Polymeric Materials, Montanuniversitaet Leoben, 8700 Leoben, Austria;* orcid.org/0000-0002-9493-3770

Christian Mitterer − *Department of Materials Science, Montanuniversitaet Leoben, 8700 Leoben, Austria*

Reinhard Pippan − *Erich Schmid Institute of Materials Science, Austrian Academy of Sciences, 8700 Leoben, Austria*

Megan J. Cordill − *Erich Schmid Institute of Materials Science, Austrian Academy of Sciences, 8700 Leoben, Austria; Department of Materials Science, Montanuniversitaet Leoben, 8700 Leoben, Austria*

Complete contact information is available at: https://pubs.acs.org/10.1021/acsanm.0c02182

Notes

The authors declare no competing financial interest.

■ ACKNOWLEDGMENTS

A.L. is funded by the Austrian Science Fund (FWF) within the Hertha Firnberg Program (T891-N36). Part of this work was carried out with the support of CEITEC Nano Research Infrastructure supported by MEYS CR (LM2018110). The authors would also like to acknowledge Helmholtz Zentrum Berlin for the allocation of synchrotron radiation beam time and thankfully acknowledge the financial support of Helmholtz Zentrum Berlin (project 17205962-ST-1.1-P).

■ REFERENCES

(1) Nix, W. D. Mechanical Properties of Thin Films. *Metall. Trans. A* **1989**, *20*, 2217−2245.

(2) Dehm, G.; Arzt, E. In Situ Transmission Electron Microscopy Study of Dislocations in a Polycrystalline Cu Thin Film Constrained by a Substrate. *Appl. Phys. Lett.* **2000**, *77*, 1126−1128.

(3) Mittal, K. L. Adhesion Measurement of Thin Films. *Electrocompon. Sci. Technol.* **1976**, *3*, 21−42.

(4) Griffits, A. A. VI. The Phenomena of Rupture and Flow in Solids. *Philos. Trans. R. Soc., A* **1921**, *221*, 163−198.
(5) Lane, M. Interface Fracture. *Annu. Rev. Mater. Res.* **2003**, *33*, 29−54.
(6) Evans, A. G.; Hutchinson, J. W.; Wei, Y. Interface Adhesion: Effects of Plasticity and Segregation. *Acta Mater.* **1999**, *47*, 4093−4113.
(7) Evans, A. G.; Rühle, M.; Dalgleish, B. J.; Charalambides, P. G. The Fracture Energy of Bimaterial Interfaces. *Metall. Trans. A* **1990**, *21*, 2419−2429.
(8) Kriese, M. D.; Moody, N. R.; Gerberich, W. W. Effects of Annealing and Interlayers on the Adhesion Energy of Copper Thin Films to SiO2/Si Substrates. *Acta Mater.* **1998**, *46*, 6623−6630.
(9) Volinsky, A. A.; Moody, N. R.; Gerberich, W. W. Interfacial Toughness Measurements for Thin Films on Substrates. *Acta Mater.* **2002**, *50*, 441−466.
(10) Khanna, V. K. Adhesion-Delamination Phenomena at the Surfaces and Interfaces in Microelectronics and MEMS Structures and Packaged Devices. *J. Phys. D: Appl. Phys.* **2010**, *44*, 034004.
(11) Tymiak, N. I.; Volinsky, A. A.; Gerberich, W. W.; Kriese, M. D.; Downs, S. A. The Role of Plasticity in Bimaterial Fracture with Ductile Interlayers. *Metall. Mater. Trans. A* **2000**, *31*, 863−872.
(12) Mittal, K. L. The Role of the Interface in Adhesion Phenomena. *Polym. Eng. Sci.* **1977**, *17*, 467−473.
(13) Dundurs, J. Discussion: "Edge-Bonded Dissimilar Orthogonal Elastic Wedges Under Normal and Shear Loading" (Bogy, D. B., 1968, ASME J. Appl. Mech., 35, pp. 460-466). *J. Appl. Mech.* **1969**, *36*, 650−652.
(14) Litteken, C. S.; Strohband, S.; Dauskardt, R. H. Residual Stress Effects on Plastic Deformation and Interfacial Fracture in Thin-Film Structures. *Acta Mater.* **2005**, *53*, 1955−1961.
(15) Dauskardt, R. H.; Lane, M.; Ma, Q.; Krishna, N. Adhesion and Debonding of Multi-Layer Thin Film Structures. *Eng. Fract. Mech.* **1998**, *61*, 141−162.
(16) Cordill, M. J.; Moody, N. R.; Bahr, D. F. The Effects of Plasticity on Adhesion of Hard Films on Ductile Interlayers. *Acta Mater.* **2005**, *53*, 2555−2562.
(17) Souli, I.; Terziyska, V. L.; Keckes, J.; Robl, W.; Zechner, J.; Mitterer, C. Effect of Growth Conditions on Interface Stability and Thermophysical Properties of Sputtered Cu Films on Si with and without WTi Barrier Layers. *J. Vac. Sci. Technol., B: Nanotechnol. Microelectron.: Mater., Process., Meas., Phenom.* **2017**, *35*, 022201.
(18) Fugger, M.; Plappert, M.; Schäffer, C.; Humbel, O.; Hutter, H.; Danninger, H.; Nowottnick, M. Comparison of WTi and WTi(N) as Diffusion Barriers for Al and Cu Metallization on Si with Respect to Thermal Stability and Diffusion Behavior of Ti. *Microelectron. Reliab.* **2014**, *54*, 2487−2493.
(19) Putz, B.; Milassin, G.; Butenko, Y.; Völker, B.; Gammer, C.; Semprimoschnig, C.; Cordill, M. J. Interfacial Mutations in the Al-Polyimide System. *Surf. Interface Anal.* **2018**, *50*, 579−586.
(20) Ritchie, R. O.; Cannon, R. M.; Dalgleish, B. J.; Dauskardt, R. H.; McNaney, J. M. Mechanics and Mechanisms of Crack Growth at or near Ceramic-Metal Interfaces: Interface Engineering Strategies for Promoting Toughness. *Mater. Sci. Eng., A* **1993**, *166*, 221−235.
(21) Oh, T. S.; Rödel, J.; Cannon, R. M.; Ritchie, R. O. Ceramic/Metal Interfacial Crack Growth: Toughening by Controlled Microcracks and Interfacial Geometries. *Acta Metall.* **1988**, *36*, 2083−2093.
(22) Hutchinson, J. W.; Suo, Z. Mixed Mode Cracking in Layered Materials. In *Advances in Applied Mechanics*; Hutchinson, J. W., Wu, T. Y., Eds.; Academic Press Incorporated, 1991; Vol. *29*, pp 63−191.
(23) Dauskardt, R. H.; Lane, M.; Ma, Q.; Krishna, N. Adhesion and Debonding of Multi-Layer Thin Film Structures. *Eng. Fract. Mech.* **1998**, *61*, 141−162.
(24) Evans, A. G.; Dalgleish, B. J. The Fracture Resistance of Metal-Ceramic Interfaces. *Acta Metall. Mater.* **1992**, *40*, S259−S306.
(25) Ruffini, A.; Finel, A.; Colin, J.; Durinck, J. Effect of Interface Plasticity on Circular Blisters. *Scr. Mater.* **2016**, *113*, 222−225.
(26) Ruffini, A.; Durinck, J.; Colin, J.; Coupeau, C.; Grilhé, J. Buckling-Induced Dislocation Emission in Thin Films on Substrates. *Int. J. Solid Struct.* **2013**, *50*, 3717−3722.
(27) Kleinbichler, A.; Zechner, J.; Cordill, M. J. Buckle Induced Delamination Techniques to Measure the Adhesion of Metal Dielectric Interfaces. *Microelectron. Eng.* **2017**, *167*, 63−68.
(28) Lassnig, A.; Nakamura, N.; Jörg, T.; Reeja-Jayan, B.; Cordill, M. J. Molecularly Grafted, Structurally Integrated Multifunctional Polymer Thin Films with Improved Adhesion. *Surf. Coating. Technol.* **2018**, *349*, 963−968.
(29) Jörg, T.; Cordill, M. J.; Franz, R.; Kirchlechner, C.; Többens, D. M.; Winkler, J.; Mitterer, C. Thickness Dependence of the Electro-Mechanical Response of Sputter-Deposited Mo Thin Films on Polyimide: Insights from in Situ Synchrotron Diffraction Tensile Tests. *Mater. Sci. Eng., A* **2017**, *697*, 17−23.
(30) Többens, D. M.; Zander, S. KMC-2: An X-Ray Beamline with Dedicated Diffraction and XAS Endstations at BESSY II. *J. large-scale Res. Facil.* **2016**, *2*, 1−6.
(31) Wern, H.; Koch, N.; Maas, T. Self-consistent Calculation of the X-Ray Elastic Constants of Polycrystalline Materials for Arbitrary Crystal Symmetry. *Mater. Sci. Forum* **2002**, *404−407*, 127−132.
(32) Oliver, W. C.; Pharr, G. M. An Improved Technique for Determining Hardness and Elastic Modulus Using Load and Displacement Sensing Indentation Experiments. *J. Mater. Res.* **1992**, *7*, 1564−1583.
(33) Tabor, D. *The Hardness of Metals*; Oxford university press: London, 1951; Vol. *75*.
(34) Marshall, D. B.; Evans, A. G. Measurement of Adherence of Residually Stressed Thin Films by Indentation. I. Mechanics of Interface Delamination. *J. Appl. Phys.* **1984**, *56*, 2632−2638.
(35) Kriese, M. D.; Gerberich, W. W.; Moody, N. R. Quantitative Adhesion Measures of Multilayer Films: Part I. Indentation Mechanics. *J. Mater. Res.* **1999**, *14*, 3007−3018.
(36) Kleinbichler, A.; Pfeifenberger, M. J.; Zechner, J.; Moody, N. R.; Bahr, D. F.; Cordill, M. J. New Insights into Nanoindentation-Based Adhesion Testing. *JOM* **2017**, *69*, 2237−2245.
(37) Bagchi, A.; Evans, A. G. Measurements of the Debond Energy for Thin Metallization Lines on Dielectrics. *Thin Solid Films* **1996**, *286*, 203−212.
(38) Kriese, M. D.; Gerberich, W. W.; Moody, N. R. Quantitative Adhesion Measures of Multilayer Films: Part II. Indentation of W/Cu, W/W, Cr/W. *J. Mater. Res.* **1999**, *14*, 3019−3026.
(39) Cordill, M. J.; Bahr, D. F.; Moody, N. R.; Gerberich, W. W. Recent Developments in Thin Film Adhesion Measurement. *IEEE Trans. Device Mater. Reliab.* **2004**, *4*, 163−168.
(40) Biesinger, M. C. Advanced Analysis of Copper X-Ray Photoelectron Spectra. *Surf. Interface Anal.* **2017**, *49*, 1325−1334.
(41) Wang, X.; Zhang, B.; Zhang, W.; Yu, M.; Cui, L.; Cao, X.; Liu, J. Super-Light Cu@Ni Nanowires/Graphene Oxide Composites for Significantly Enhanced Microwave Absorption Performance. *Sci. Rep.* **2017**, *7*, 1584.
(42) Cordill, M. J.; Muppidi, T.; Moody, N. R.; Bahr, D. F. Effects of Microstructure on the Mechanical Properties of Copper Films for High Aspect Ratio Structures. *Microsyst. Technol.* **2004**, *10*, 451−455.
(43) Atkins, A. G.; Mai, Y.-W. *Elastic and Plastic Fracture*, 1st edn; Ellis Horwood Limited: Chichester, 1985.